FINITE ELEMENT SIMULATION OF ANISOTROPIC DAMAGE AROUND PRESSURIZED BOREHOLES IN PREFRACTURED SHALE

W. Jin, H. Xu, C. Arson
School of Civil & Environmental Engineering, Georgia Institute of Technology
wencheng.jin@gatech.edu, haoxu@gatech.edu, chloe.arson@ce.gatech.edu

ABSTRACT

Optimizing hydraulic fracture injection parameters in order to maximize hydrocarbon extraction and to avoid extensive borehole spalling is still an open issue. In this paper, the Differential Stress Induced Damage (DSID) model is employed to simulate the anisotropic damage distribution around pressurized boreholes drilled in fractured shale. The loading path is purely mechanical: excavation and fluid injection are simulated by stress relaxation followed by pressurization. We investigate the effect of pre-existing fracture orientation, in-situ stress and injection pressure on the propagation of anisotropic damage during pressurization. Finite Element results indicate that (1) damage initiates and develops when the ratio of two in-situ stress component deviates from 1, and the magnitude of damage is proportional to this stress deviation; (2) For a given in-situ stress field, damage initiates for a certain threshold of injection pressure, and the damage zone extends as the injection pressure increases; (3) A pre-existing fracture only affects the damage zone locally; the orientation of that fracture does not affect the damaged zone, which is controlled by in situ stress and injection pressure.

KEYWORDS

Anisotropic damage, Hydraulic pressure, In-situ stress, Fracture orientation

INTRODUCTION

Hydraulic fracturing is used to increase shale permeability and to enhance hydrocarbon extraction. In order to maximize the extraction ratio and to avoid wellbore spalling and clogging during fluid injection, the parameters related to injection for each particular site need to be optimized. Therefore, it is necessary to clearly understand how shale responses upon excavation and pressurization.

It is well known that breakouts grow in the direction of minimum compression and that plastic deformation around wellbores tends to arrest breakouts (Zoback et al., 1985). Laboratory acoustic emission tests revealed that fractures propagate along the direction of maximum compression stress, and fractures (breakouts) are surrounded by the Excavation Damaged Zone (EDZ), in which rock properties are weakened by the presence of micro cracks (Eberhardt et al., 1999; Martino et al., 2004). The anisotropy from orientated foliations and cracks may influence the development and propagation of fractures and breakouts (Everitt et al., 2004). Sonic televiewer logs proved that during hydraulic fracturing, fluid injection further alters the stress distribution (Evans et al., 2005). Shale natural fabric strongly affects the evolution of the EDZ around boreholes.

In this paper, we investigate the effect of pre-existing fracture orientation, in-situ stress and injection pressure on the propagation of anisotropic damage during hydraulic fracturing. The Differential Stress Induced Damage (DSID) model (Xu and Arson, 2014) used in this study is presented in the first section. Section 2 explains how the DSID model was calibrated to Bakken shale laboratory data. Section 3 summarizes Finite Element simulations conducted to analyze the sensitivity of stress and damage to in situ stress, injection pressure and pre-existing fracture orientation.

THEORETICAL FRAMEWORK OF THE DISD MODEL

We study anisotropic damage evolution around wellbores with the DSID model (Xu & Arson, 2014). The damage variable is a second order tensor (denoted Ω), which is used to model the distribution of micro-crack planes present in a Representative Elementary Volume (REV) of rock (Fig.1a). Gibbs free energy G_s is expressed as follows:

$$G_s(\boldsymbol{\sigma},\boldsymbol{\Omega}) = \frac{1}{2}\boldsymbol{\sigma}:\mathrm{S}_0:\boldsymbol{\sigma} + a_1\mathrm{Tr}\boldsymbol{\Omega}\left(\mathrm{Tr}\boldsymbol{\sigma}\right)^2 + a_2\mathrm{Tr}\left(\boldsymbol{\sigma}\cdot\boldsymbol{\sigma}\cdot\boldsymbol{\Omega}\right) + a_3\mathrm{Tr}\boldsymbol{\sigma}\mathrm{Tr}\left(\boldsymbol{\Omega}\cdot\boldsymbol{\sigma}\right) + a_4\mathrm{Tr}\boldsymbol{\Omega}\mathrm{Tr}\left(\boldsymbol{\sigma}\cdot\boldsymbol{\sigma}\right) \quad (1)$$

Where a_i are material parameters (determined from numerical calibration in the next section). S_0 is the initial undamaged compliance fourth-order tensor. The total deformation tensor is split as

$$\boldsymbol{\varepsilon} = \boldsymbol{\varepsilon}^{el} + \boldsymbol{\varepsilon}^{ed} + \boldsymbol{\varepsilon}^{id} = \boldsymbol{\varepsilon}^{E} + \boldsymbol{\varepsilon}^{id} \quad (2)$$

In which $\boldsymbol{\varepsilon}^{el}$ is the purely elastic strain, $\boldsymbol{\varepsilon}^{ed}$ is the elastic damage-induced strain that result from the degradation of mechanical stiffness, and $\boldsymbol{\varepsilon}^{id}$ is the irreversible strain. A hyper-elastic framework is adopted. Accordingly, the thermodynamic conjugation relationships are:

$$\begin{aligned}\boldsymbol{\varepsilon}^{E} = \boldsymbol{\varepsilon} - \boldsymbol{\varepsilon}^{id}\left(\boldsymbol{\Omega}\right) = \frac{\partial G_s}{\partial\boldsymbol{\sigma}} = \frac{1+\nu_0}{E_0}\boldsymbol{\sigma} - \frac{\nu_0}{E_0}\left(\mathrm{Tr}\boldsymbol{\sigma}\right)\boldsymbol{\delta} + 2a_1\left(\mathrm{Tr}\boldsymbol{\Omega}\mathrm{Tr}\boldsymbol{\sigma}\right)\boldsymbol{\delta}\frac{1}{2} \\ + a_2\left(\boldsymbol{\sigma}\cdot\boldsymbol{\Omega}+\boldsymbol{\Omega}\cdot\boldsymbol{\sigma}\right) + a_3\left[\mathrm{Tr}\left(\boldsymbol{\Omega}\cdot\boldsymbol{\sigma}\right)\boldsymbol{\delta} + \left(\mathrm{Tr}\boldsymbol{\sigma}\right)\boldsymbol{\Omega}\right] + 2a_4\left(\mathrm{Tr}\boldsymbol{\Omega}\right)\boldsymbol{\sigma}\end{aligned} \quad (3)$$

$$\mathbf{Y} = \frac{\partial G_s}{\partial\boldsymbol{\Omega}} = a_1\left(\mathrm{Tr}\boldsymbol{\sigma}\right)^2\boldsymbol{\delta} + a_2\boldsymbol{\sigma}\cdot\boldsymbol{\sigma} + a_3\left(\mathrm{Tr}\boldsymbol{\sigma}\right)\boldsymbol{\sigma} + a_4\mathrm{Tr}\left(\boldsymbol{\sigma}\cdot\boldsymbol{\sigma}\right)\boldsymbol{\delta} \quad (4)$$

Where E_0 and ν_0 are Young's modulus and Poisson ratio of initial undamaged material. $\boldsymbol{\delta}$ is the identity tensor. The damage criterion is similar to a Drucker Prager yield function expressed in terms of energy release rate, in order to predict the evolution of damage with deviatoric stress:

$$\begin{aligned} & f_d = \sqrt{J^*} - \alpha I^* - k \\ & J^* = \frac{1}{2}\left(\mathrm{P}_1:\mathbf{Y}\text{-}\frac{1}{3}I^*\boldsymbol{\delta}\right):\left(\mathrm{P}_1:\mathbf{Y}\text{-}\frac{1}{3}I^*\boldsymbol{\delta}\right), \qquad I^* = \left(\mathrm{P}_1:\mathbf{Y}\right):\boldsymbol{\delta} \\ & \mathrm{P}_1\left(\boldsymbol{\sigma}\right) = \sum_{p=1}^{3}\left[H\left(\sigma^{(p)}\right) - H\left(-\sigma^{(p)}\right)\right]\boldsymbol{n}^{(p)}\otimes\boldsymbol{n}^{(p)}\otimes\boldsymbol{n}^{(p)}\otimes\boldsymbol{n}^{(p)} \\ & k = C_0 - C_1\mathrm{Tr}(\boldsymbol{\Omega}) \end{aligned} \quad (5)$$

C_0 is the initial damage threshold, C_1 is an isotropic hardening variable, $H(\cdot)$ is the Heaviside function and $\sigma^{(p)}$ is the p-th principal stress. The irreversible strain is calculated from an associated flow rule as:

$$\dot{\boldsymbol{\varepsilon}}^{id} = \dot{\boldsymbol{\lambda}}_d\frac{\partial f_d}{\partial\boldsymbol{\sigma}} = \dot{\boldsymbol{\lambda}}_d\frac{\partial f_d}{\partial\mathbf{Y}}:\frac{\partial\mathbf{Y}}{\partial\boldsymbol{\sigma}}. \quad (6)$$

In order to satisfy the positivity of dissipation, the damage flow rule is chosen as non-associate:

$$\dot{\boldsymbol{\Omega}} = \dot{\boldsymbol{\lambda}}_d\frac{\partial g_d}{\partial\mathbf{Y}}, \quad (7)$$

In which $\dot{\boldsymbol{\lambda}}_d$ is the Lagrangian Multiplier, and:

$$\begin{aligned} & g_d = \sqrt{\frac{1}{2}\left(\mathrm{P}_2:\mathbf{Y}\right):\left(\mathrm{P}_2:\mathbf{Y}\right)} \\ & \mathrm{P}_2\left(\boldsymbol{\sigma}\right) = \sum_{p=1}^{3}H\left[\max_{q=1}^{3}\left(\sigma^{(p)}\right) - \sigma^{(p)}\right]\boldsymbol{n}^{(p)}\otimes\boldsymbol{n}^{(p)}\otimes\boldsymbol{n}^{(p)}\otimes\boldsymbol{n}^{(p)} \end{aligned} \quad (8)$$

PARAMETRIC CALIBTRATION FOR SHALE

Shale is a sedimentary rock transformed from extremely compact clay. Parallel bedding planes formed during the deposition process provide natural anisotropy. Samples of North Dakota Bakken Shale were prepared so as to ensure material statistical homogeneity. Triaxial compression tests performed by

ConocoPhillips rock mechanics laboratory are used as reference. We wrote an iterative algorithm based on the least-square to calibrate the DSID model. The main governing equations are as follows:

$$S = \sum_{i=1}^{n} r_i^2, \qquad r_i = y_i - f\left(\boldsymbol{x}, \boldsymbol{B}\right)$$
$$\boldsymbol{B}_{n+1} = \boldsymbol{B}_n - \gamma_n \mathrm{d}f\left(\boldsymbol{B}_n\right) \tag{9}$$

S is the residual distance between experimental results y_i and numerical predictions $f\left(\boldsymbol{x}, \boldsymbol{B}\right)$. $\boldsymbol{x}$ is the vector of input data (e.g., strain for a displacement-controlled test, stress for a force-controlled test). $\boldsymbol{B}$ is the vector of unknown parameters: calculated to minimize S. Parameters found for North Dakota Bakken shale are listed in Table 1.

Table 1: Calibrated DSID parameters for Bakken shale

Elasticity		Free energy				Damage function		
E	v	a_1	a_2	a_3	a_4	C_0	C_1	α
GPa	-	GPa^{-1}	GPa^{-1}	GPa^{-1}	GPa^{-1}	MPa	MPa	-
46	0.186	7.35×10^{-4}	0.121	-3.15×10^{-2}	2.39×10^{-3}	0.01	1.18	0.399

NUMERICAL ANALYSIS OF STRESS AND DAMAGE ANISOTROPY

We simulated the pressurization of a horizontal borehole drilled in fractured shale with the Finite Element method. Plane strain was assumed. We modeled a pre-existing fracture as a 0.1m-thick shale layer with an initial damage equal to 20% in the direction orthogonal to the fracture plane (Fig.1). We chose an in situ stress range in which the rock behaves elastically during the excavation phase. Damage occurred during the pressurization phase (Fig.2). The stress applied as the cavity wall during the first phase of the loading was calculated according to the following elastic stress distributions (Brady & Brown, 2004):

$$\sigma_{rr} = \frac{K+1}{2} p + \frac{K-1}{2} p \cos 2\theta$$
$$\sigma_{r\theta} = -\frac{K-1}{2} p \sin 2\theta \tag{10}$$

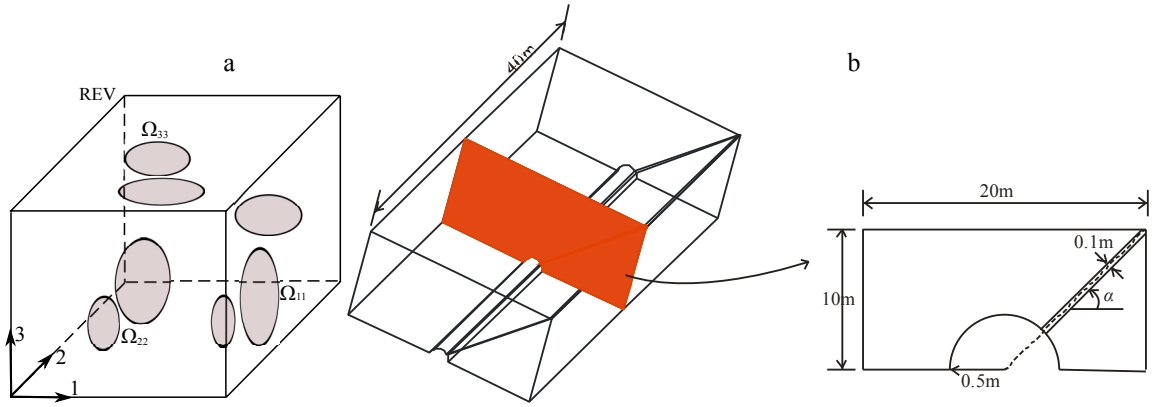

Figure 1. (a) Sketch of the damage components (b) Geometry of simulation domain in the FE Analysis

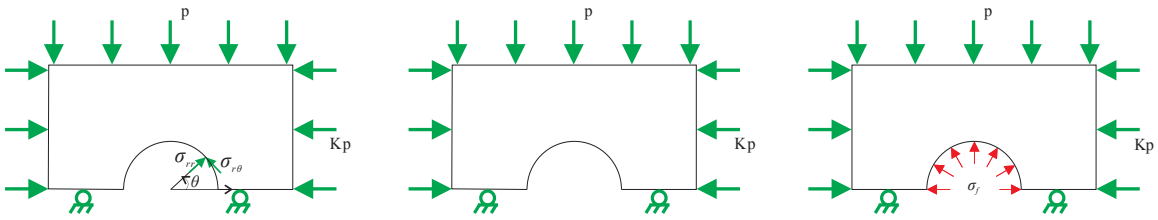

Figure 2. Boundary conditions adopted in the parametric studies (in sit stress, excavation, pressurization)

Table 2: Simulation plan for the parametric studies

Simulation cases	Orientation of damage layer	Vertical load	Horizontal coefficient	Injection pressure
	(°)	p (MPa)	K (-)	σ_f (MPa)
Far field stress control	30	20	0.5,0.75,1,1.25,1.5,1.75	50
Hydraulic pressure control	45	20	0.5	10,20,30,40,50,60
Fracture orientation control	0,15,30,45,60,75,90	10	0.5	50

Effect of in-situ stress anisotropy

We simulated borehole pressurization for the six in situ stress states summarized in Table 2. The pre-existing fracture orientation was fixed at 30° to the horizontal, the vertical in situ stress was 20MPa, and the pressure applied at the wall was 50MPa. According to the theory of elasticity (Brady and Brown, 2004), the stress around a circular hole of radius R embedded in an infinite medium subjected to a uniform internal pressure σ_f, a vertical far field stress p and a horizontal far field stress Kp is given by:

$$\sigma_{rr} = \frac{1}{2}p(1+K)(1-\frac{R^2}{r^2}) - \frac{1}{2}p(1-K)(1-4\frac{R^2}{r^2}+3\frac{R^4}{r^4})\cos(2\theta) + \sigma_f\frac{R^2}{r^2}$$
$$\sigma_{\theta\theta} = \frac{1}{2}p(1+K)(1+\frac{R^2}{r^2}) + \frac{1}{2}p(1-K)(1+3\frac{R^4}{r^4})\cos(2\theta) - \sigma_f\frac{R^2}{r^2} \quad (11)$$

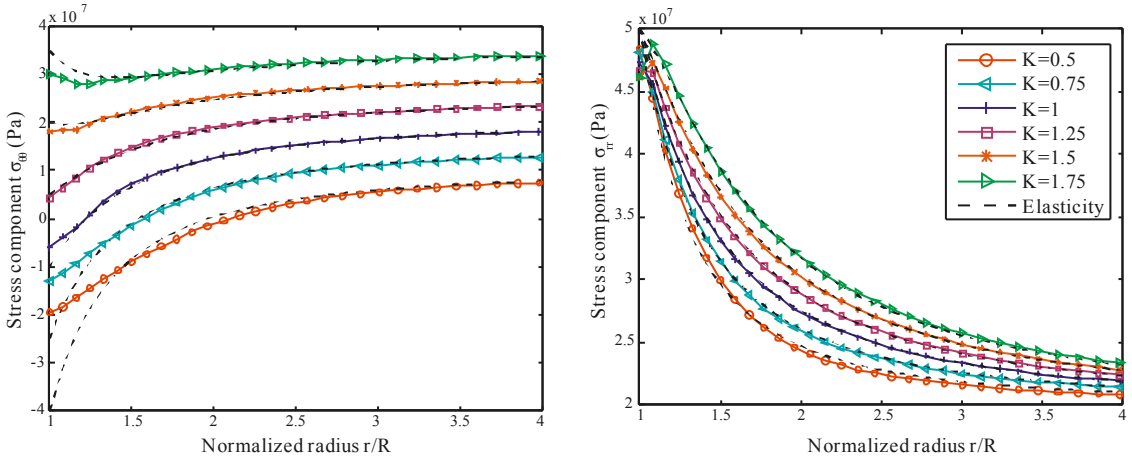

Figure 3. Radial distribution of stress ($\alpha = 30^\circ$, $\theta = \pi/2$, $r = 0.5 - 2m$) for different in situ stress ratios: comparison of the DSID prediction with the elastic stress distribution.

Fig.3 shows that the radial distribution of stress in the vertical direction (θ=π/2) gets closer to the analytical stress distribution when the stress ratio K approaches 1. In the far field, numerical and analytical stress distributions are identical, which means that damage only occurs at the vicinity of the cavity wall (within a zone equal to 1.5R), as confirmed by the damage distribution plots shown in Fig.4. When $K<1$, the tensile hoop stress initiate micro vertical cracks, which results in damage in horizontal direction (Ω_{11}). Shale elements experience higher strain and lower stress than the pure elastic case. The intensity of Ω_{11} diminishes quickly as r increases and $K \to 1$. When $K>1$, the difference between

horizontal and vertical compression stress initiates vertical damage, i.e. horizontal micro-cracks (Fig.1.a), which results in damage in the vertical direction (Ω_{22}).

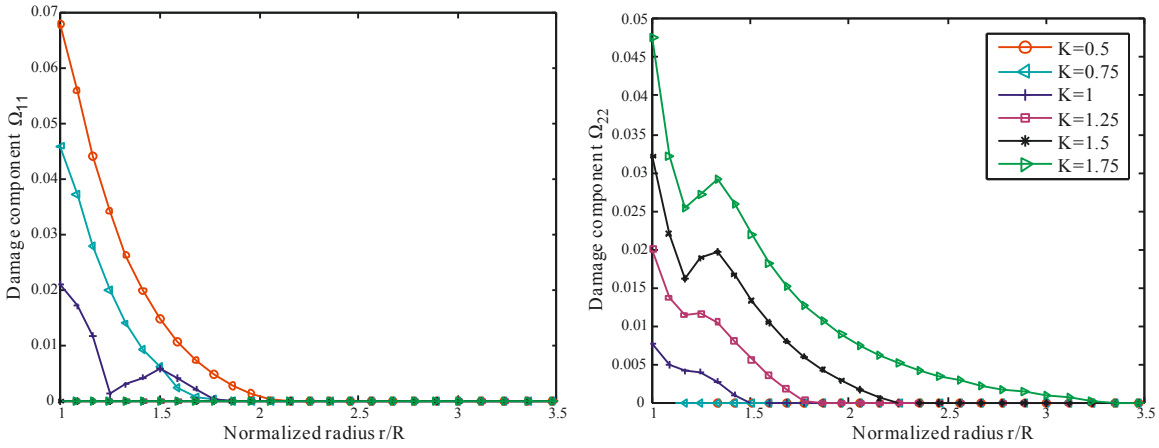

Figure 4. Radial distribution of damage ($\alpha = 30^{\circ}, \theta = \pi/2, r = 0.5 - 1.75m$) for different in situ stress ratios.

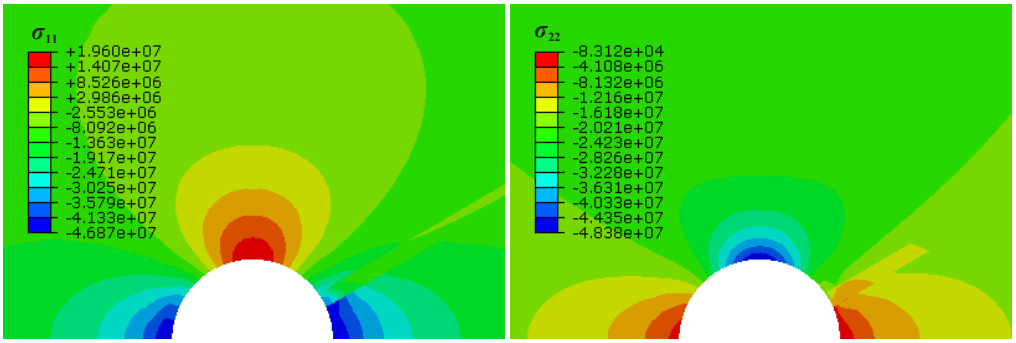

Figure 5. Distribution of horizontal (left) and vertical (right) stress after a pressurization of $\sigma_f = 50MPa$ in shale subjected to a confining pressure of $p = 20MPa, K = 0.5$ in the far field. Note: in the FEM program, compression was counted negative and tension was counted positive.

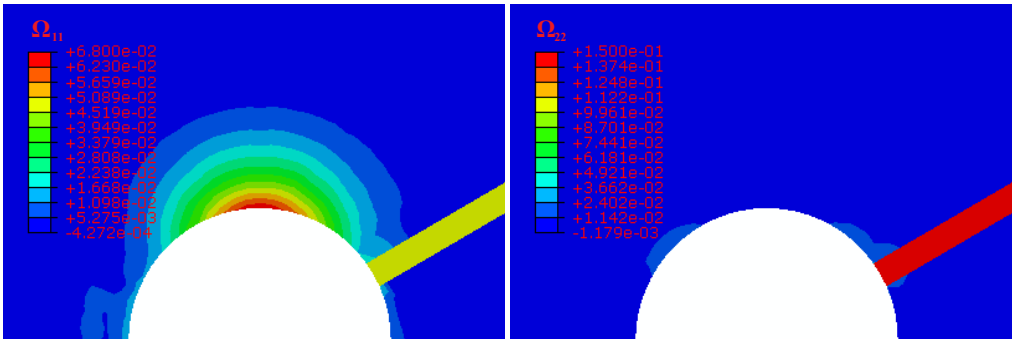

Figure 6. Distribution of horizontal (left) and vertical (right) damage after a pressurization of $\sigma_f = 50MPa$ in shale subjected to a confining pressure of $p = 20Mpa, K = 0.5$ in the far field. Note that by definition, damage eigenvalues cannot be negative, but components of the damage tensor can be negative.

Figures 5 and 6 show the state of stress and damage around the borehole with $K=0.5$. Tensile and compression stresses follow a symmetric distribution around the borehole except for the area close to the pre-existing fracture, around which tensile stress tends to concentrate. Vertical micro-cracks (i.e. horizontal damage Ω_{11}) propagate at the crown. Damage increases in the zone that represents the pre-existing fracture.

Effect of the injection pressure

We simulated borehole pressurization for the six injection pressures summarized in Table 2. The pre-existing fracture orientation was fixed at 45° to the horizontal, the vertical in situ stress was 20MPa, and the horizontal in situ stress was 10MPa. Fig.7 shows the radial stress distribution in the vertical direction (θ=π/2). For injection pressures inferior to 30MPa, numerical predictions match the analytical stress distribution, which indicates that shale remains elastic. When $\sigma_f \geq 30MPa$, the hoop stress close to the cavity decreases due to material softening. In other words, micro cracks initiate and develop as the hydraulic pressure increases, which results in a deviation from the elastic solution. Note that damage propagation has a negligible influence on radial stress distribution compared to that on the hoop stress.

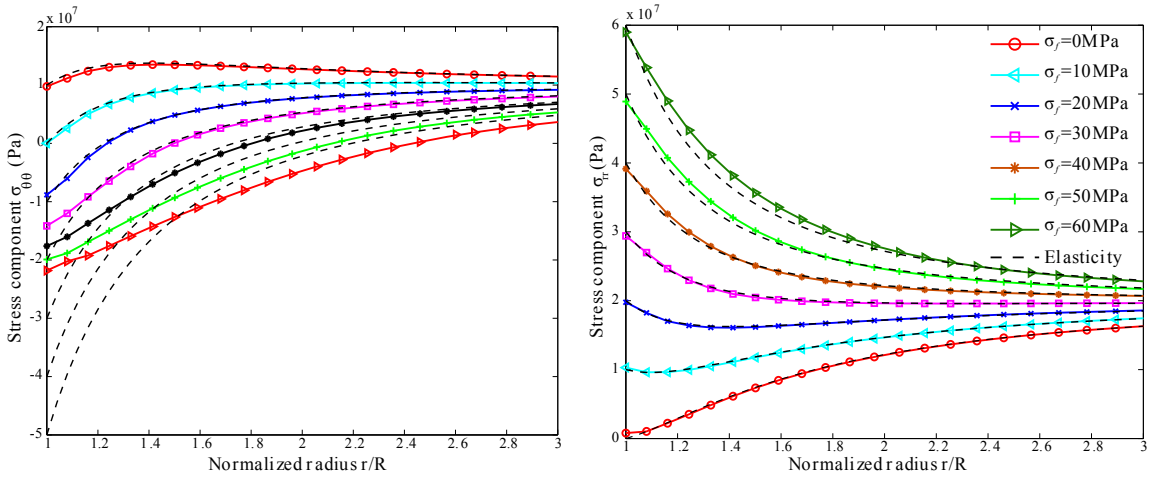

Figure 7. Radial distribution of stress ($p=20MPa$, $K=0.5$, $\alpha=45°$, $\theta=\pi/2$, $r=0.5-1.5m$) for different injection pressures: comparison of the DSID prediction with the elastic stress distribution.

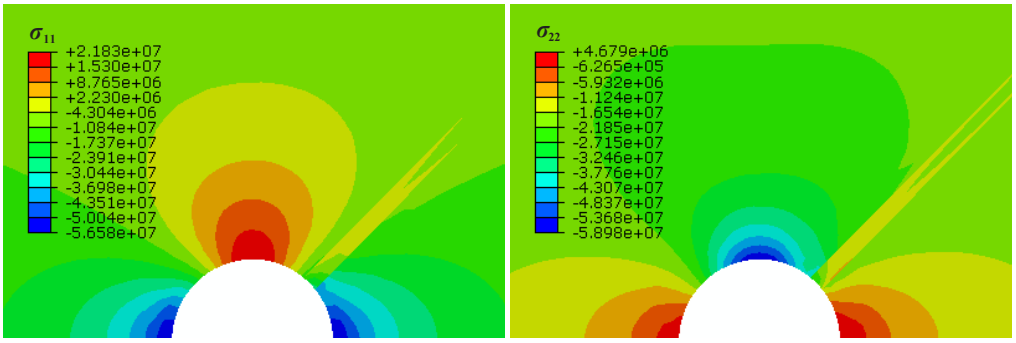

Figure 8. Distribution of horizontal (left) and vertical (right) stress in the whole domain near the cavity, after a pressurization $\sigma_f = 60MPa$ under a confining pressure of $p=20Mpa, K=0.5$ in the far field.

Note: in the FEM program, compression was counted negative and tension was counted positive.

Fig.8 and (d, e, f) of Fig.9 show the state of stress and damage in the vicinity of the cavity after a pressurization of 60MPa under a confining stress of p=20MPa, $K=0.5$. All the components of stress and damage are symmetric, except near the pre-damaged layer. Inside the pre-existing fracture, initial damage softens the material, which leads to lower compression stress. At the crown, high vertical compression and

high horizontal tension originate vertical cracks (horizontal damage, Ω_{11} – see Fig.9(d)). The pre-existing fracture redistributes shear damage, which concentrates in a narrow zone oriented by an angle of 45˚ to the horizontal (Fig.9(e)). Figure 9 also shows that the magnitude and extent of damage zone increases proportionally with hydraulic pressure and that compared to vertical macro cracks, the intensity of shear damage Ω_{12} and vertical damage Ω_{22} is less than 1% that of horizontal damage Ω_{11}.

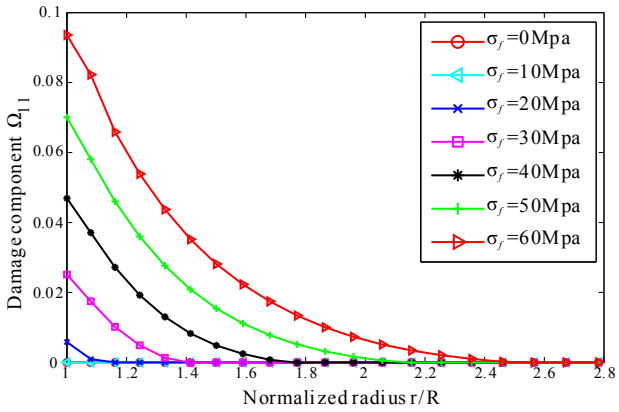

(a)

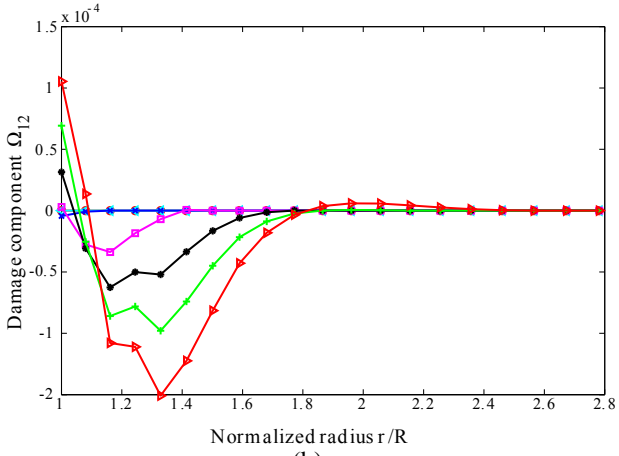

(b)

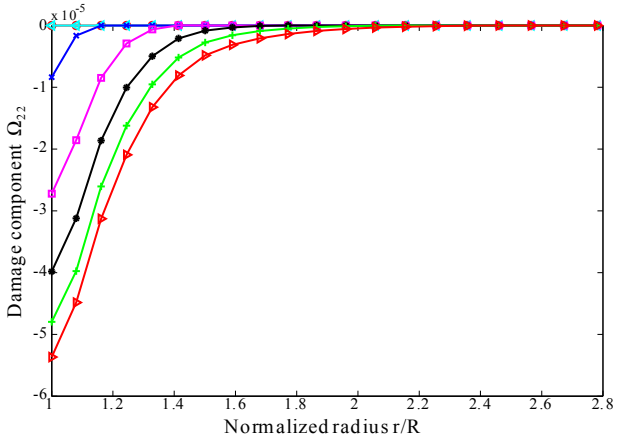

(c)

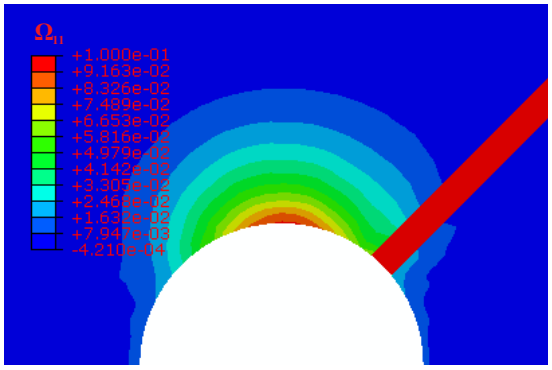

(d) Damage component in the horizontal direction Ω_{11} (vertical micro-cracks)

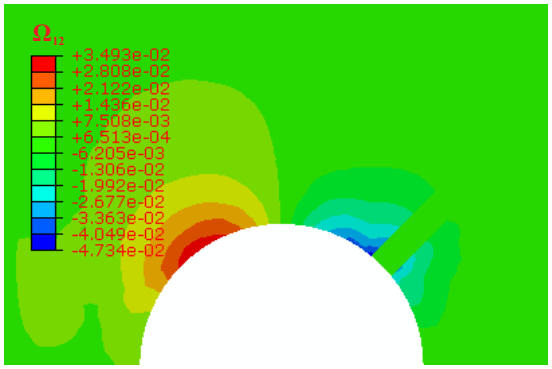

(e) Shear damage Ω_{12}

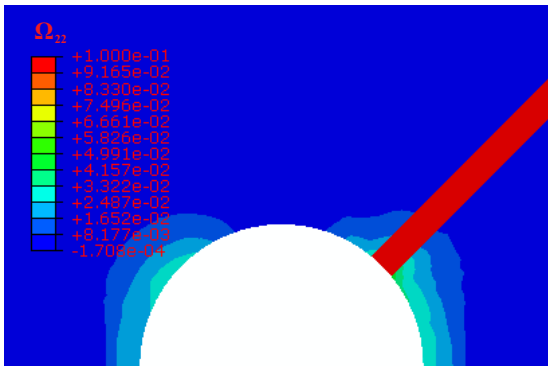

(f) Damage component in the vertical direction Ω_{22} (horizontal micro-cracks)

Figure 9. Radial distribution of damage components (a- Ω_{11} , b- Ω_{12} , c- Ω_{22}) in the vertical direction ($\theta = \pi/2$) for increased hydraulic pressures σ_p ; Damage distribution (d, e, f) around the cavity after a pressurization $\sigma_f = 60MPa$ subjected to a confining pressure of $p = 20MPa, K = 0.5$ in the far field.

Effect of pre-existing fracture orientation

In order to confirm the importance of the impact of the pre-existing fracture on the development of damage at the sidewalls, we simulated borehole pressurization for the six fracture orientations summarized in Table 2. The vertical in situ stress was 10MPa, the horizontal in situ stress was 5MPa, and the pressure applied at the wall was 50MPa. Fig.10 shows the radial stress distribution in the vertical direction. The orientation of fracture has negligible effect on stress distribution. For a vertical fracture ($\alpha = 90^\circ$), the radial stress plotted in the figure is in fact inside the pre-damaged zone, in which the material is softened and the stress level is lower than without pre-damage. The major vertical and minor horizontal far field stresses induce tension in the horizontal direction and compression in the vertical direction at the top of cavity. Vertical damage is negligible compared to horizontal damage (Fig.11).

Fig.12 shows that the radial stress distribution in the horizontal direction is not influenced by the orientation of the fracture, which only disturbs the stress field locally. This result confirms the observations made in Fig.10, and is further supported by the low value of the damage components at material points aligned along the horizontal direction (Fig.13).

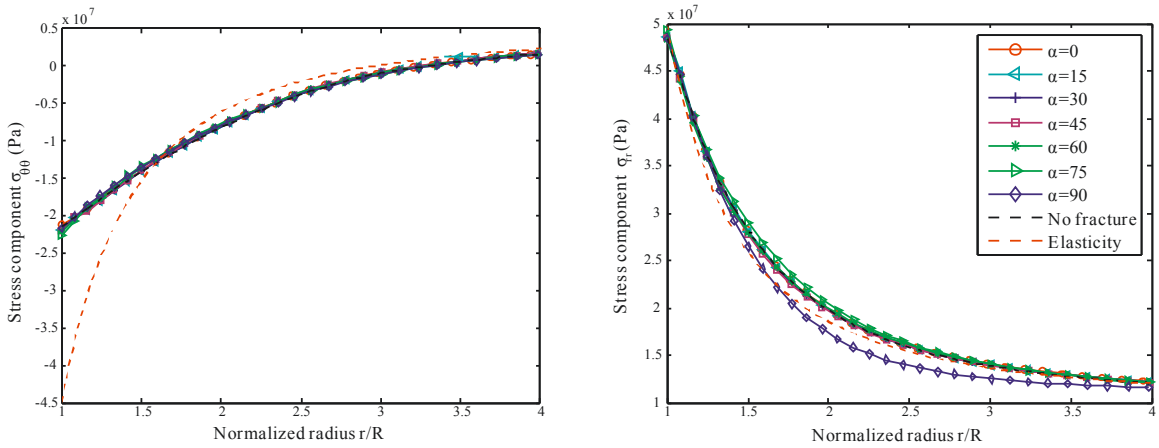

Figure 10. Radial distribution of stress along the vertical direction ($p = 10MPa$, $K = 0.5$, $\sigma_f = 50MPa$, $\theta = \pi/2$, $r = 0.5 - 2m$) for different orientations of the pre-existing fracture: comparison of the DSID prediction with the elastic stress distribution. Note: the pre-existing fracture was modeled by Finite Elements with an initial damage of 20% in the direction normal to the fracture plane.

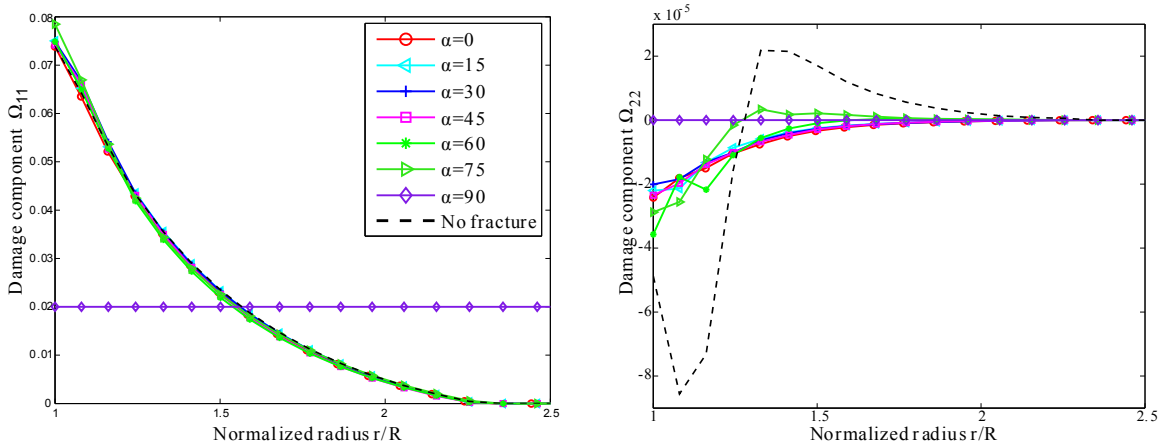

Figure 11. Radial distribution of horizontal (left) and vertical (right) damage along the vertical direction ($p = 10MPa$, $K = 0.5$, $\sigma_f = 50MPa$, $\theta = \pi/2$, $r = 0.5 - 1.25m$) for different orientations of the pre-existing fracture. Note: the pre-existing fracture was modeled by Finite Elements with an initial damage of 20% in the direction normal to the fracture plane.

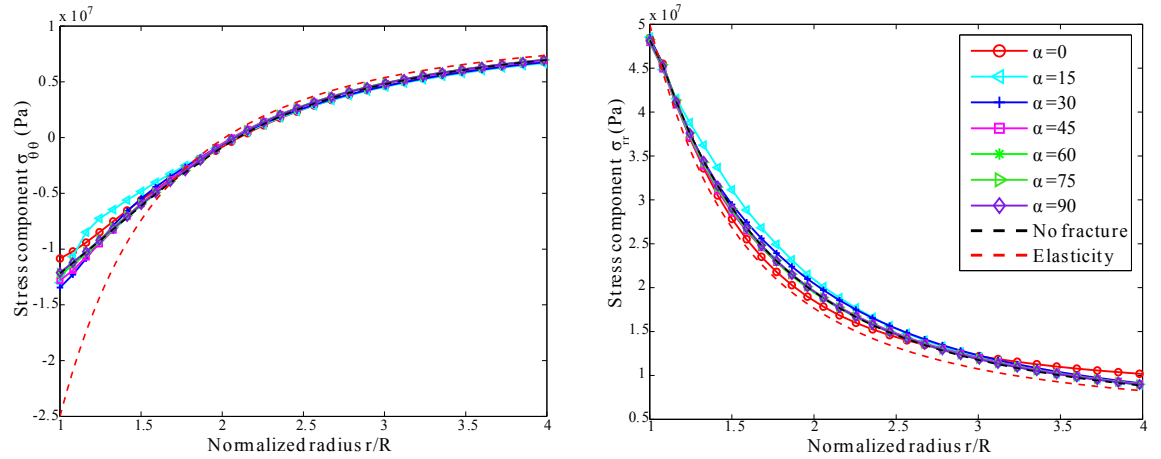

Figure 12. Radial distribution of stress along the horizontal direction ($p = 10MPa$, $K = 0.5$, $\sigma_f = 50MPa$, $\theta = 0$, $r = 0.5 - 2m$) for different orientations of the pre-existing fracture: comparison of the DSID prediction with the elastic stress distribution. Note: the pre-existing fracture was modeled by Finite Elements with an initial damage of 20% in the direction normal to the fracture plane.

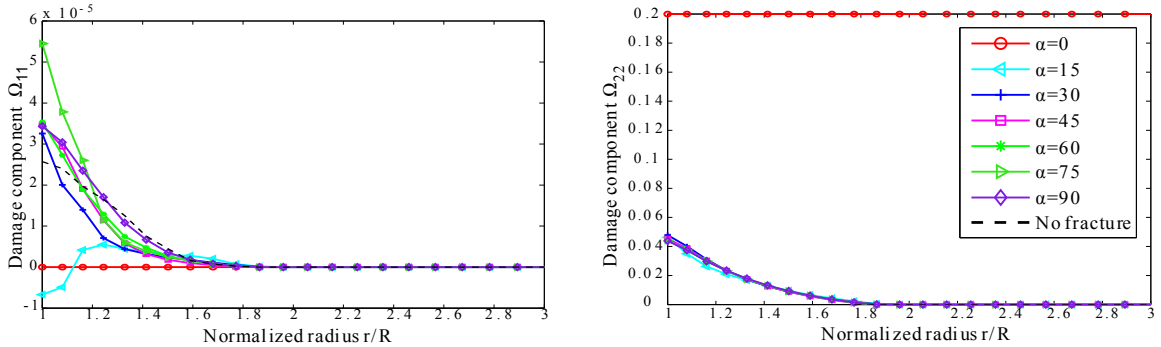

Figure 13. Radial distribution of horizontal (left) and vertical (right) damage along the horizontal direction ($p = 10MPa$, $K = 0.5$, $\sigma_f = 50MPa$, $\theta = 0$, $r = 0.5 - 1.5m$) for different orientations of the pre-existing

fracture. Note: the pre-existing fracture was modeled by Finite Elements with an initial damage of 20% in the direction normal to the fracture plane.

CONCLUSIONS

We used the Differential Stress Induced Damage model (DSID model) to study the sensitivity of anisotropic damage propagation around a pressurized borehole to in situ stress anisotropy, injection pressure and pre-existing fractures. The damage criterion is similar to Drucker–Prager yield function. A damage potential is introduced in order to account for non-elastic damaged deformation. We calibrated the DSID model against experimental data obtained for North Dakota Bakken shale. We performed a parametric study with the Finite Element Method. The main results are the following:

1) The hoop stress distribution departs from the elastic stress distribution due to the propagation of damage at the vicinity of the borehole. Past a certain threshold of injection pressure (30 MPa in the particular case treated in the paper), the difference between the elastic and the damaged stress distributions increases when the in situ stress anisotropy increases. Radial stress is practically not influenced by damage.
2) The intensity of damage and the extent of the damaged zone in the vertical direction increase with the injection pressure and with the relative far field stress ratio $|K-1|$.
3) The orientation of a pre-existing fracture has a negligible effect on the propagation of damage around the borehole, except locally: in situ stress and injection pressure control the damaged zone.

ACKNOWLEDGEMENTS

Authors' research sponsors are Georgia Tech School of Civil and Environmental Engineering, Georgia Tech Offices of the Provost and Executive Vice President for Research, and ConocoPhillips.

REFERENCES

Brady, B. H., Brown, E.T. (2004). Rock mechanics: for underground mining. Springer.

Everitt, R. and Lajtai, E. (2004). The influence of rock fabric on excavation damage in the lac du bonnett granite. International Journal of Rock Mechanics & Mining Sciences, vol. 41, pp. 1277–1303.

Eberhardt, E., Stead, D., & Stimpson, B. (1999). Quantifying progressive pre-peak brittle fracture damage in rock during uniaxial compression. International Journal of Rock Mechanics and Mining Sciences, 36(3), 361-380.

Evans, K. F., Genter, A., & Sausse, J. (2005). Permeability creation and damage due to massive fluid injections into granite at 3.5 km at Soultz: 1. Borehole observations. Journal of Geophysical Research: Solid Earth (1978–2012), 110(B4).

Martino, J. B., & Chandler, N. A. (2004). Excavation-induced damage studies at the underground research laboratory. International Journal of Rock Mechanics and Mining Sciences, 41(8), 1413-1426.

Xu, H., & Arson, C. (2014). Anisotropic Damage Models for Geomaterials: Theoretical and Numerical Challenges. International Journal of Computational Methods, 11(02).

Zoback, M. D., Moos, D., Mastin, L., & Anderson, R. N. (1985). Well bore breakouts and in situ stress. Journal of Geophysical Research: Solid Earth (1978–2012), 90(B7), 5523-5530.